JOURNAL OF SPACECRAFT AND ROCKETS
Vol. 41, No. 6, November–December 2004

Approximate Method to Estimate Wing Trailing-Edge Bluntness Effects on Normal Force

F. G. Moore*
Aeroprediction, Inc., King George, Virginia 22485
and
T. C. Hymer†
U.S. Naval Surface Warfare Center, Dahlgren, Virginia 22448

A new semiempirical method has been developed to estimate the effect of wing trailing-edge bluntness on configuration normal force and center of pressure. The new method has been integrated into the aeroprediction code (APC) and will be a part of the next release in 2005 (AP05). Comparison of the new method for several cases where experimental data were available showed that the modified version of the AP05 gave improved predictions of aerodynamics compared to the 2002 version of the APC (AP02) and experiment. In addition to improvements in normal force and center of pressure, some improvement in axial force at transonic and subsonic speeds was also made for wings with truncated leading or trailing edges. The axial force improvements were based on improved two-dimensional base pressure coefficients and a simple method to estimate the axial force of a truncated wing leading edge.

Nomenclature

A_{BLE}	=	area of blunt leading edge of wing, ft^2
AR	=	aspect ratio
A_{ref}	=	reference area, ft^2
b	=	wing span, not including body diameter, ft
C_A	=	axial force coefficient
C_{L_α}	=	lift coefficient derivative, rad^{-1}
$(C_{L_\alpha})_0$	=	lift coefficient derivative with sharp trailing-edge fins, rad^{-1}
C_{M_α}	=	pitching moment coefficient derivative, rad^{-1}
C_N	=	normal force coefficient
C_{N_α}	=	normal force coefficient derivative, rad^{-1}
C_P, C_{P_0}	=	pressure and stagnation pressure coefficient, respectively
$C_{P_{2\text{-}D}}$	=	two-dimensional base pressure coefficient
C_1, C_2	=	constants used in second-order theory
c, c_r, c_t	=	chord, root, and tip chord, respectively, ft
c_n	=	local chordwise normal force coefficient
d	=	body diameter, ft
h	=	wing trailing-edge height, ft
M_∞	=	freestream Mach number
N_F	=	number of fins
P, P_t	=	pressure and total pressure, respectively
r_{LE}, r_{TE}	=	leading- and trailing-edge radius of wing, respectively, ft
r_n	=	body nose tip radius, ft
s	=	distance from wedge leading edge to first discontinuity downstream, ft
t, t_r, t_t	=	thickness, root chord, and tip chord thickness of wing, respectively, ft
X_{CP}/d	=	center of pressure, calibers from some reference point
α	=	angle of attack, deg
β	=	rear portion of wedge half-angle, deg
γ	=	ratio of specific heats of air
δ	=	angle between velocity vector and tangent to a local point on the body or wing surface, deg
δ_W	=	wedge half-angle, deg
θ	=	shock wave angle, deg
λ	=	wing taper ratio, c_t/c_r
ν	=	Prandtl–Meyer expansion angle, deg

Introduction

THIS paper describes a new semiempirical method to estimate the effects of blunting the trailing edge of fins on the normal force and pitching moment coefficient derivatives at low angles of attack (AOA). In addition, improvements in axial force of the wings were developed for wings that had either truncated leading or trailing edges. The new methods will be integrated into a future version of the aeroprediction code (APC). The latest version of the APC available to users is the 2002 version, or the AP02.[1] The AP02 takes into account wing-thickness and trailing-edge bluntness effects on the axial force of the wing, as well as the effect of wing thickness on the body base pressure. No account is taken of the added wing axial force at subsonic and transonic speeds if the wing leading edge is truncated. Also, for the low AOA normal force coefficient derivative of wings, the AP02 assumes that the wing is infinitely thin at both supersonic and subsonic Mach numbers. Some effect of thickness is taken into consideration empirically at transonic speeds.

The motivation behind the incorporation of leading- and trailing-edge bluntness effects into the APC is driven by the desire to estimate more accurately the axial force and normal force coefficient slope and static stability of guided projectiles at high launch velocities. Many guided projectiles are constrained in length, and with the desire to increase range, any improvements in static stability at high Mach numbers is important. Reference 2 showed a consistent improvement in normal force coefficient slope of wings at low AOA, with the percent increase in C_{N_α} increasing with increasing supersonic Mach numbers.

A typical guided projectile concept is shown by the wind-tunnel model of Fig. 1. The concept in Fig. 1 utilizes eight tail fins to get as much static stability at launch as possible. Because the Fig. 1 fins fold rearward at launch to fit within the gun barrel and because additional fin span would take away from rocket propellant and,

Received 1 May 2003; revision received 21 October 2003; presented as Paper 2004-16 at the Aerospace Sciences Meeting, Reno, NV, 5 January 2004; accepted for publication 26 January 2004.

*President, 9449 Grover Drive, Suite 201; drfgmoore@hotmail.com. Associate Fellow AIAA.

†Aerospace Engineer, Weapons Systems Department, Missile Systems Division, Dahlgren Division. Member AIAA.

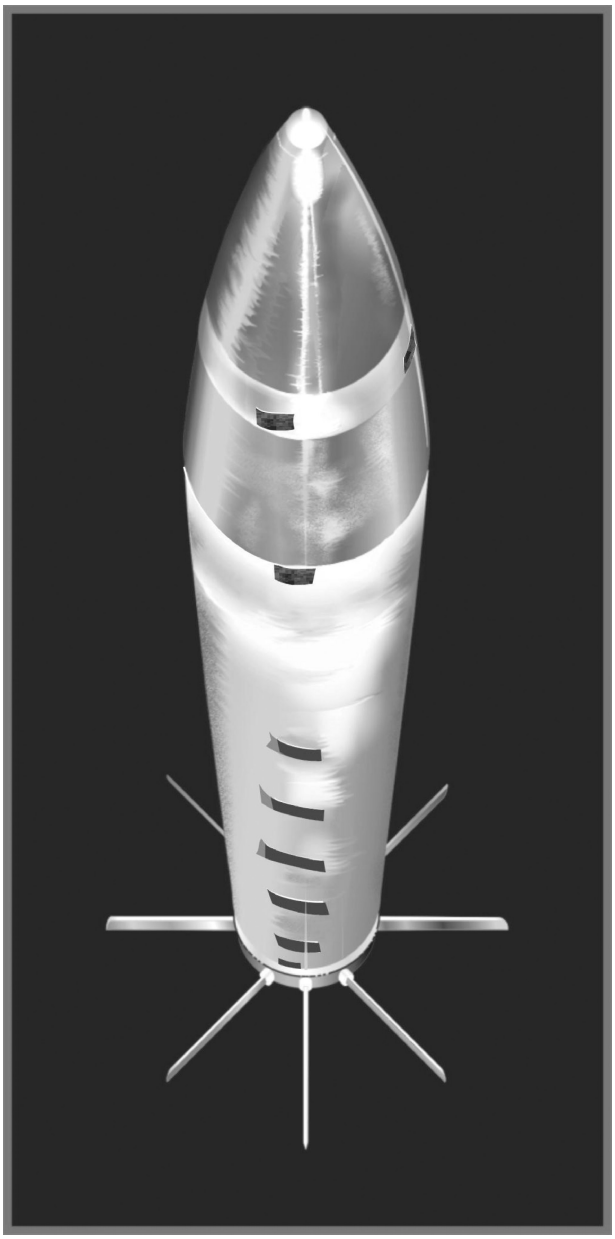

Fig. 1 Wind-tunnel model of guided projectile configuration with eight fins.

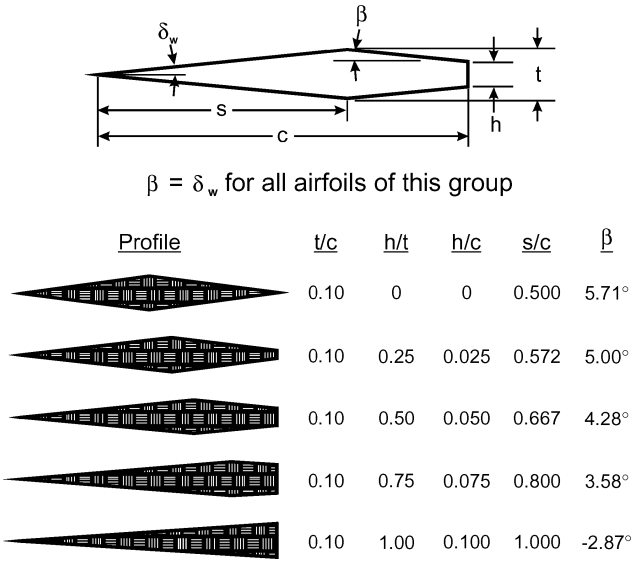

Fig. 2a Profiles of wedge as double wedge airfoils (taken from Ref. 2).

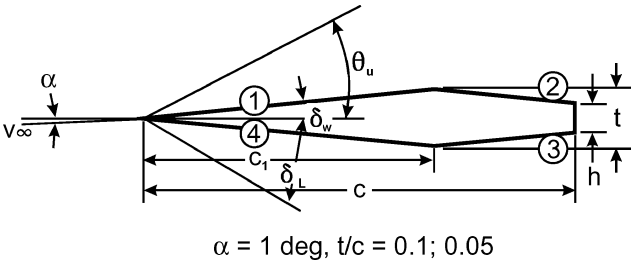

Fig. 2b Supersonic flow over a two-dimensional airfoil.

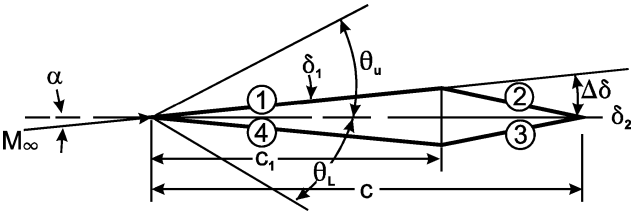

Fig. 2c Supersonic flow over wedge and turning angle.

hence, range, it is highly desirable to get as much static stability at launch as possible. Even 0.1–0.50-caliber improvement in static margin at high Mach number is considered significant. It was for this reason that Aeroprediction, Inc. (API), was tasked by the U.S. Naval Surface Warfare Center, Dahlgren Division (NSWCDD) to develop a simple, yet reasonably accurate, method to compute the increase in static margin on a weapon due to trailing-edge bluntness effects and then to integrate this new method into the APC.

In searching the literature for both data and methods to compute normal force effects due to trailing-edge bluntness, several reports were found, written primarily in the late 1940s and early 1950s (Refs. 2–6). In addition, several references dealt with the trailing-edge thickness effects on drag.[7–10] Figure 2a shows examples of airfoils considered in Ref 2. It is clear in viewing these references that it was known in the 1950s time frame that trailing-edge thickness of wings led to higher normal force coefficients compared to sharp trailing-edge fins.[2–6] Also, the axial force coefficients were also reduced at moderate to high supersonic Mach numbers when the trailing edge was blunt compared to a sharp trailing-edge.[7–10]

The question that one is naturally left with is, because both the normal force and axial force coefficients can show improvement when blunt trailing-edge airfoils are used vs sharp trailing-edge wings, why are blunt trailing-edge wings not used on more modern-day weapons? The first author speculates there are several reasons for this. First, during the time frame when the trailing-edge effect became known, most weapons flew at subsonic to low supersonic Mach numbers. Hence, whereas the axial force can be reduced for moderate to high supersonic Mach numbers with blunt vs sharp trailing-edge airfoils, it is increased for subsonic to low supersonic speeds. The increase in axial force coefficient at Mach numbers 1.5 and lower for blunt trailing-edge wings is suspected to be the main reason for the use of sharp trailing-edge fins. Second, fins are very effective as a lifting device at moderate supersonic speeds and lower: thus, a small increase in normal force may not be that important. Third, if the fins were used for control, placement of the control arm near the midchord of the wing would keep the hinge moments to a minimum. The control arm location generally required the wing thickness to be a maximum at that point. Finally, the higher speed requirements of future guided projectiles has only come about in the last few years. This higher speed requirement has caused a new look at ways to get increased static margin at high supersonic to low hypersonic Mach numbers. This was not a requirement 50 years ago.

It is, therefore, the purpose of this paper to develop an approximate method that can be used to estimate rapidly the effects of

trailing-edge thickness on the normal force and pitching moment coefficients of wings. During development of the new method for normal force coefficient for blunt-trailing edge fins, it was noticed that improvements in fix axial force were needed at transonic and subsonic Mach numbers. Improvements in fin axial force coefficient were, therefore, developed along with normal force coefficient improvements. The new methods can then be integrated into the next version of the APC, the AP05. The AP02 currently does a reasonably good job of predicting the axial force coefficient of wings at all Mach numbers greater than 1.3. Blunt leading or trailing edges, aspect ratio, sweepback, variable thickness along the wing span, and effect of fins on body base drag are all included in the AP02 wing axial force methodology. Hence, the wing axial force methodology will be modified only for Mach numbers below 1.3. Interested readers are referred to Ref. 11 for the details of the wing alone methodology for computing axial force coefficient. To summarize the Ref. 11 methods briefly, first-order perturbation theory plus modified Newtonian theory is used for wave drag, the Van Driest II method is used for skin-friction drag, and empirical methods are used for body base drag, trailing-edge thickness drag, and wing thickness effects on body base drag.

Analysis

Chapman and Kester[2] discussed the two primary theoretical methods to compute the change in either axial or normal force of two-dimensional airfoils. These are the second-order theory of Buseman and Walchmer[5] and shock-expansion theory (SET). The SET, when applied to sharp leading-edge airfoils at supersonic speeds high enough to give an attached shock, can actually be an exact theory for wedge or double-wedge airfoil shapes. These two methods will be briefly outlined, followed by a new semiempirical approach that utilizes results from the SET along with experimental data or extrapolations outside the range of validity for the SET.

Second-Order Theory

The second-order theory (SOT), according to Buseman and Walchmer,[5] gives a pressure coefficient on the airfoil surface as

$$C_P = C_1\delta + C_2\delta^2 \tag{1}$$

where δ is the angle between the tangent to a local point on the airfoil surface, and the freestream velocity and C_1 and C_2 are constants given by

$$C_1 = \frac{2}{\sqrt{M_\infty^2 - 1}}, \qquad C_2 = \frac{(\gamma+1)M_\infty^4 - 4\left(M_\infty^2 - 1\right)}{2\left(M_\infty^2 - 1\right)^2} \tag{1a}$$

Both Refs. 5 and 9 showed that if one integrates the pressure coefficient over the airfoil surface from Eq. (1) and compares the lift curve slope of a double wedge airfoil with trailing-edge bluntness to that with no bluntness, the increase in lift curve slope can be written as

$$\frac{C_{L_\alpha} - \left(C_{L_\alpha}\right)_0}{\left(C_{L_\alpha}\right)_0} = \frac{2C_1[1 + (C_2/C_1)(h/c)] - 2C_1}{2C_1} \tag{2}$$

By the use of relations (1a), Eq. (2) becomes

$$\frac{C_{L_\alpha} - \left(C_{L_\alpha}\right)_0}{\left(C_{L_\alpha}\right)_0} = \frac{h}{c}\left[\frac{(\gamma+1)M_\infty^4 - 4\left(M_\infty^2 - 1\right)}{4\left(M_\infty^2 - 1\right)^{\frac{3}{2}}}\right] \tag{3}$$

Equation (3) indicates that the increase in lift curve slope is directly proportional to the airfoil base thickness to chord ratio (h/c), independent of the airfoil profile ahead of the base, as well as being a function of freestream Mach number.

SET

To apply SET to a sharp leading-edge airfoil, we must first determine the flow properties behind an attached shock. For a two-dimensional airfoil at AOA, the flow properties are different on the upper and lower surface, and so one must solve for the shock angle on the upper surface and then the shock angle on the lower surface. With knowledge of the shock angle for the upper and lower surfaces, all flow properties across the shock can be determined and are constant between the shock and the wedge tip of the airfoil surface. Mathematically, if the upper surface slope with respect to the freestream is δ_1, and the lower surface slope with respect to the freestream is δ_4 (Fig. 2b), then

$$\delta_1 = \delta_W - \alpha, \qquad \delta_4 = \delta_W + \alpha \tag{4}$$

Also, from Ref. 12, the shock wave angle $\theta_{1,4}$ for the upper and lower surfaces is found from the numerical solution of

$$\sin^6(\theta_{1,4}) + a\sin^4(\theta_{1,4}) + \mathrm{d}\sin^2(\theta_{1,4}) + e = 0 \tag{5}$$

where

$$a = -\left[\left(M_\infty^2 + 2\right)/M_\infty^2\right] - \gamma\sin^2(\delta_{1,4})$$

$$d = 2\left[\left(M_\infty^2 + 1\right)/M_\infty^4\right] + \left[(\gamma+1)^2/4 + (\gamma-1)/M_\infty^2\right]\sin^2(\delta_{1,4})$$

$$e = -\cos^2(\delta_{1,4})/M_\infty^2$$

With $\theta_{1,4}$ known from Eq. (5), then,

$$\frac{P_{1,4}}{P_\infty} = \frac{2\gamma M_\infty^2\sin^2(\theta_{1,4}) - (\gamma-1)}{\gamma+1} \tag{6}$$

$$C_{P_{1,4}} = \frac{2}{\gamma M_\infty^2}\left[\frac{P_{1,4}}{P_\infty} - 1\right] \tag{7}$$

$$M_{1,4}^2 = \left[\frac{M_\infty^2\sin^2(\theta_{1,4}) + 5}{7M_\infty^2\sin^2(\theta_{1,4}) - 1}\right]\left[\frac{1}{\sin^2(\theta_{1,4} - \delta_{1,4})}\right] \tag{8}$$

Equations (6–8) determine the required flow properties at the leading edge of the sharp two-dimensional airfoil with an attached shock. To determine the value of the flow properties at the next point downstream, we use Prandtl–Meyer (PM) expansion. First, we determine the PM angle $\nu_{1,4}$ that corresponds to the Mach number $M_{1,4}$ from

$$\nu_{1,4} = \sqrt{(\gamma+1)/(\gamma-1)}\tan^{-1}\left\{\sqrt{[(\gamma-1)/(\gamma+1)]\left(M_{1,4}^2 - 1\right)}\right\} - \tan^{-1}\sqrt{M_{1,4}^2 - 1} \tag{9}$$

If $\Delta\delta$ (Fig. 2c) is the change in the local surface slope in going from point (1,4) on the airfoil leading edge to the next point (2, 3) downstream, then

$$\nu_{2,3} = \Delta\delta + \nu_{1,4} \tag{10}$$

$M_{2,3}$ is then determined numerically from Eq. (9).

Note that if we have a simple double wedge, then

$$\nu_{2,3} = 2\delta_W + \nu_{1,4} \tag{10a}$$

and the flow properties are constant on all four surfaces of the wedge if the shock is attached. With $M_{2,3}$ known, then,

$$P_{t_{2,3}}/P_{2,3} = \left\{1 + [(\gamma-1)/2]M_{2,3}^2\right\}^{\gamma/(\gamma-1)} \tag{11}$$

$$P_{t_{1,4}}/P_1 = \left\{1 + [(\gamma-1)/2]\,M_{1,4}^2\right\}^{\gamma/(\gamma-1)} \tag{12}$$

$$P_{2,3}/P_\infty = \left(P_{t_{1,4}}/P_{1,4}\right)\left(P_{2,3}/P_{t_{2,3}}\right)(P_{1,4}/P_\infty) \tag{13}$$

$$C_{P_{2,3}} = \left(2/\gamma M_\infty^2\right)(P_{2,3}/P_\infty - 1) \tag{14}$$

Equations (9–14) are applied all along the airfoil surface, so that the upper and lower surface pressure coefficients are all known. Integrations of the pressure coefficients over the airfoil surface will give the normal force coefficient from Eq. (15):

$$c_n = \frac{1}{c}\int_{X_{\mathrm{LE}}}^{X_{\mathrm{TE}}} \left(C_{P_L} - C_{P_U}\right) \mathrm{d}x \tag{15}$$

or, for the entire wing, from Eq. (16),

$$C_N = \frac{2}{A_{\mathrm{ref}}}\int_0^{b/2} cc_n \,\mathrm{d}y \tag{16}$$

Note that because AOA is included in Eq. (4), Eq. (16) will be a function of AOA. However, it is not as straightforward to obtain C_{N_α} as for the SOT of Eqs. (2) and (3).

Figures 3a and 3b compare the SOT of Eq. (3) to the SET of Eqs. (7–14) for a double wedge (C_{L_0}) compared to a wedge (C_L) of thickness-to-chord ratio of 0.05 (Fig. 3a) and 0.10 (Fig. 3b). The SET results of Fig. 3 were taken from Ref. 2. Note that the

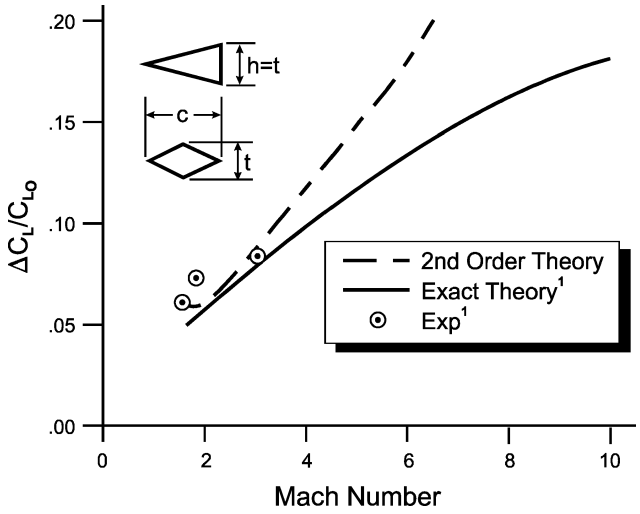

Fig. 3a Theoretical lift increment of wedge airfoil ($h/c = 0.05$) relative to double wedge airfoil ($h/c = 0$).

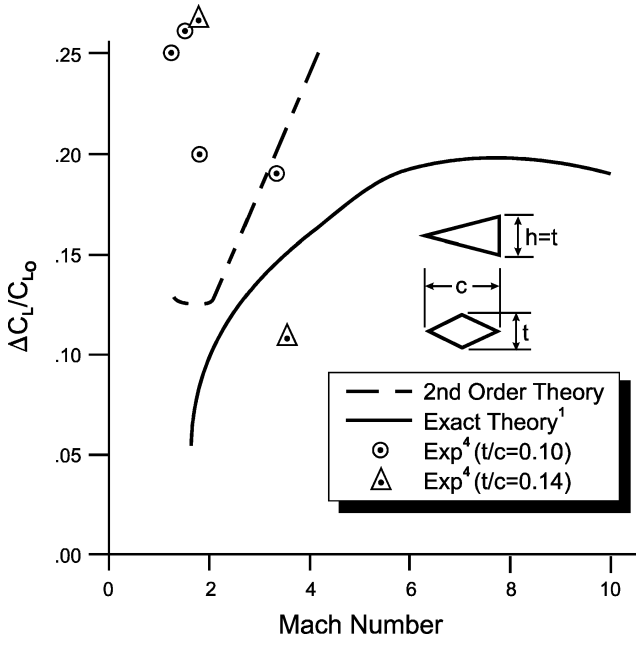

Fig. 3b Theoretical lift increment of wedge airfoil ($h/c = 0.1$) relative to double wedge airfoil ($h/c = 0$).

percent increase in lift for the wedge compared to the double wedge increases substantially as Mach numbers increases. Second, the SOT deviates substantially from the SET as Mach number increases. The SOT assumes isentropic flow, whereas the SET is an exact theory for both the wedge and double wedge. Hence, the SET is the more accurate of the methods. Third, although the $h/c = 0.1$ case percent increase in lift for the wedge compared to the double wedge is higher for most Mach numbers than that for the $h/c = 0.05$ case, the value of the lift increase for $h/c = 0.1$ is not twice that of $h/c = 0.05$ at any Mach number. In fact, at high Mach numbers, the percent increase in lift for the wedge over the double wedge appears to reach a plateau of about equal value for the values of $h/c = 0.05$ and 0.10. Finally, note that no values are given for lower Mach numbers, where SET becomes invalid due to a detached shock.

Semi-Empirical Theory

Reference 2 gave a simple formula to estimate the effect of trailing-edge thickness on the lift curve slope with engineering accuracy as

$$C_{L_\alpha} = \left(C_{L_\alpha}\right)_0 [1 + 1.2\,(h/c)] \tag{17}$$

Chapman[2] indicated that Eq. (17) was a first approximation to the trailing-edge thickness effects for wings of aspect ratio greater than one, for Mach numbers between 1.5 and 3.1, and for turbulent flow on the wings. The wings that were tested also had a sharp leading edge and were rectangular. Equation (17) basically says that the lift coefficient slope at small AOA for a wing with trailing-edge thickness is increased in a direct proportion to the trailing-edge thickness. For example, for a wing that had a 10% trailing-edge thickness ratio ($h/c = 0.1$), then Eq. (17) says that the C_{L_α} is increased by 12% over a wing with no trailing-edge thickness ($C_{L_\alpha} = 1.12C_{L_0}$).

The objective here is to derive a semiempirical expression, analogous to Eq. (17), but more general and robust in its application. To that end, we will assume

$$C_{L_\alpha} = \left(C_{L_\alpha}\right)_0 \times [1 + f_1(h/c, M) f_2(r_{\mathrm{LE}}/t) f_3(\mathcal{A}\mathrm{R}) f_4(N_F)(h/c)/(t/c)] \tag{18}$$

Basically, Eq. (18) is analogous to Eq. (17) if we assume

$$f_1(h/c, M) = (1.2)(t/c), \qquad f_2(r_{\mathrm{LE}}/t) = 1.0$$
$$f_3(\mathcal{A}\mathrm{R}) = 1.0, \qquad f_4(N_F) = 1.0 \tag{19}$$

However, to make Eq. (17) more general, we must define expressions for the values of f_1, f_2, f_3, and f_4 of Eq. (18). Another way to look at Eq. (18) is that the lift of wings with blunt trailing edges will be increased slightly over those of sharp trailing edges. The amount of the increase will be defined by the second term within the bracket of Eq. (18). The amount of the increase in lift (or pitching moment) is a function of not only the trailing-edge thickness, but Mach number, wing aspect ratio, wing leading-edge radius, and number of fins present.

The first parameter that will be defined is $f_1(h/c, M_\infty)$. The shock expansion theory of Figs. 3a and 3b (which for a double wedge or wedge airfoil is an exact inviscid theory) will be used along with some experimental data,[4] extrapolation, and engineering judgment to formulate values of the parameter f_1. Figure 4 gives the value of f_1 gleaned from a combination of Fig. 3, Ref. 4, and engineering judgment. Note that both t/c and h/c of Fig. 4 and Eq. (18) are assumed to be values at the wing root chord.

Also, because we are considering a modification of the low AOA C_{L_α} for wings based on trailing-edge thickness, we will assume that $(C_{L_\alpha})_0$ of Eq. (18) is replaced by $(C_{N_\alpha})_0$ of the AP02. The AP02 value of $(C_{N_\alpha})_0$ is calculated based on lifting surface theory subsonically, three-dimensional thin wing theory supersonically, and empirically transonically. The only region where thickness effects the AP02 value of $(C_{N_\alpha})_0$ is in the transonic speed regime, where thickness actually degrades the lift curve slope vs increasing it. As seen in Fig. 4, the exact theory also shows a sharper decline in f_1

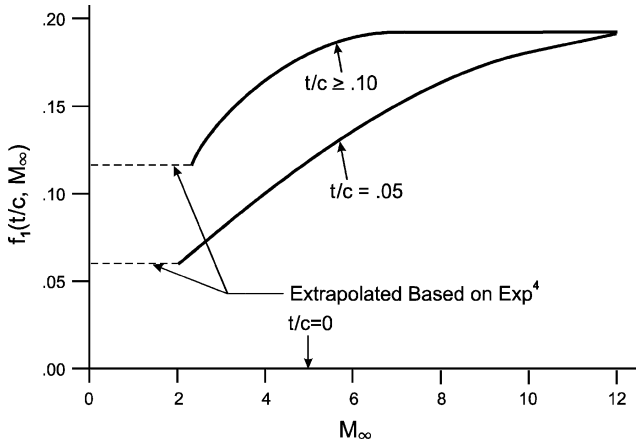

Fig. 4 Parameter use to define the additional normal force increment of a wedge compared to a double-wedge airfoil.

for $t/c = 0.1$ around $M_4 = 4.0$ than for $t/c = 0.05$. This sharp decline in f_1 of Fig. 4 for thick wings is similar to the methodology in the AP02 for transonic speeds. The AP02 value for $(C_{N_\alpha})_0$, although calculated based on a flatplate, has sweepback, aspect ratio, taper ratio, and Mach number effects already included and has been demonstrated to give reasonable accuracy for low AOA wing alone aerodynamics for many years.

In examining Fig. 4, it is seen that the SET will be used for Mach numbers of about 2 to 12 and t/c values of 0.1 and less. For t/c values above 0.1, we will assume the value of f_1 at $t/c = 0.1$ will be used, and, for Mach numbers above 12, the value at Mach number of 12 will be used. For Mach numbers below about 2, where SET may not be applicable, the experimental data of Ref. 4, along with extrapolation and engineering judgment, is used. For t/c values between 0 and 0.1, interpolation between the curves for 0.1, 0.05, and 0.0 of Fig. 4 is used for a given Mach number. The values of f_1 for $M_4 < 2.0$ are intentionally defined on the low side of the experimental data to not overestimate the effects of trailing-edge thickness. From a practical standpoint, the area of most interest in the present work is from $M_\infty = 2$ to about 8, where SET is most accurate.

The next parameter of Eq. (18) to define is $f_2(r_{\mathrm{LE}}/t)$. All of the configurations of Ref. 2 had a sharp leading edge. It appears natural to assume that if the leading edge of the airfoil is 100% blunt, then, even if the trailing edge is 100% blunt, no additional benefit should be obtained over a wing with no trailing-edge bluntness. This statement is based on the fact that SET indicates that the reason for the improvement in wing lift due to trailing-edge bluntness comes from leading- and trailing-edge wedge angles. Because the leading- and trailing-edge angles both go to zero due to leading- and trailing-edge bluntness, then it will be assumed that the factor f_2 also goes to zero. In other words, f_2 will be assumed to have the behavior

$$f_2 = (1 - 2r_{\mathrm{LE}}/t) \tag{20}$$

Once again, the root chord value of (r_{LE}/t) is used.

The third parameter one needs to determine is $f_3(\mathcal{A}\mathrm{R})$. Recall that Fig. 4 is a two-dimensional value based on an infinite aspect ratio airfoil. Also, because the wings we are interested in will, in general, be attached to the body, the finite aspect ratio actually has the wing-tip effects, as well as the wing–body effects. Figure 5 shows the wing-tip and wing–body effects that diminish the two-dimensional effects of Fig. 4. To estimate the wing-tip effects, Ref. 2 gave experimental results for $\Delta C_{L_\alpha}/(C_{L_\alpha})_0$ as a function of the wing area blanketed by the tip Mach cones. By the use of these data, and by averaging out the slopes of the curves represented by the various Mach numbers, thickness ratios, Reynolds number, and fraction of wing area blanketed by the tip Mach cones, an expression was arrived at:

$$f_3(\mathcal{A}\mathrm{R}) = 1 - \frac{0.064}{\mathcal{A}\mathrm{R}\sqrt{M_\infty^2 - 1}} \tag{21}$$

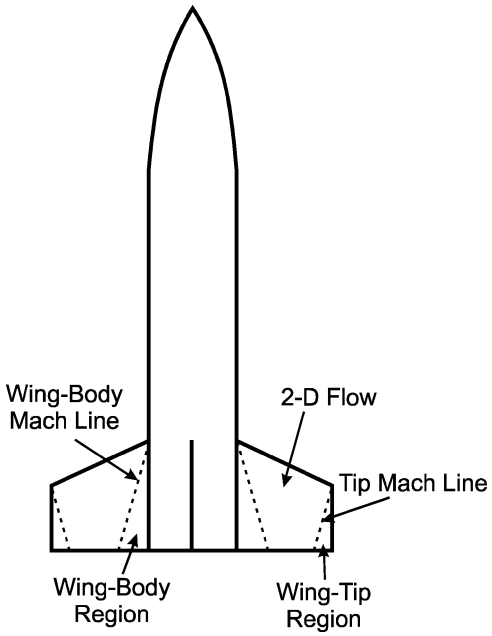

Fig. 5 Wing-tip and wing-body three-dimensional flow regions.

Because the Ref. 2 data considered only wing-tip effects of rectangular wings, it will be assumed that the constant 0.064 will be doubled to account for the wing–body effects as well. Hence,

$$f_3(\mathcal{A}\mathrm{R}) = 1 - \frac{0.128}{\mathcal{A}\mathrm{R}\sqrt{M_\infty^2 - 1}}, \qquad M_\infty \geq 1.2$$

$$f_3(\mathcal{A}\mathrm{R}) = 1, \qquad M_\infty \leq 0.8$$

$$f_3(\mathcal{A}\mathrm{R}) = (f_3)_{M=0.8} + \frac{M_\infty - 0.8}{0.4}$$

$$[(f_3)_{M=1.2} - (f_3)_{M=0.8}], \qquad 0.8 < M_\infty < 1.2 \tag{22}$$

with the constraint that if $f_3 < 0$, then $f_3 \equiv 0$.

The last parameter of Eq. (18) is $f_4(N_F)$. We will assume that f_4 is defined by the same factor determined in Ref. 13. Reference 13 used computational fluid dynamics codes to define factors for six and eight fins to multiply the wing–body and body–wing normal force coefficients of four fins. This allowed the AP02 to compute aerodynamics of six- and eight-fin weapons based on four-fin weapon aerodynamics. The values of these factors are given in Table 1 for convenience. The factor $f_4(N_F)$ would be replaced by F_6 or F_8 if six or eight fins were present, vs four fins. Table 1 extends the values of F_6 and F_8 from Ref. 13 to aspect ratio 4 cases by extrapolation. Reference 13 assumed that the aspect ratio 2 data applied for all aspect ratios greater than 2.0 as well.

Substituting Eqs. (20) and (22) into Eq. (18) along with use of Fig. 4 and Table 1 now allows one to calculate an approximate value of increase in the low AOA normal force coefficient of fins. Again, $(C_{N_\alpha})_0$ of Eq. (18) is the flat plate, wing-alone value from the AP02, and f_1 is defined by interpolation by the use of given wing parameters and Fig. 4. Equation (18) is the final expression to incorporate wing trailing-edge thickness effects into the low AOA wing lift curve slope.

As AOA gets large, the AP02 uses a fourth-order method to predict the wing normal force as a function of AOA, Mach number, aspect ratio, and taper ratio. The value of $(C_{N_\alpha})_{\alpha \approx 0}$ is one of the parameters used in the fourth-order method, but it has increasingly less importance as AOA gets larger.

Reference 3 showed that there was little change in the wing center of pressure due to wing trailing-edge thickness. Because the center of pressure of the wing alone is simply the pitching moment divided by the normal force, the implication is that wing trailing-edge bluntness affects the pitching moment similar to the normal force. Therefore, the wing alone pitching moment of the AP02 will be modified

Table 1 Approximated values of the factors F6 and F8 obtained from smoothed values of the ZEUS and GASP code computations and engineering judgement

	F_6, Mach number					F_8, Mach number				
α	0.6	1.5	2.0	3.0	4.5	0.6	1.5	2.0	3.0	4.5
					AR-0.25					
0	1.26	1.37	1.27	1.19	1.22	1.90	1.42	1.40	1.27	1.20
15	1.00	1.00	1.10	1.19	1.35	1.45	1.03	1.17	1.27	1.35
30	1.00	1.00	1.00	1.19	1.22	1.00	1.00	1.01	1.27	1.22
45	1.00	1.00	1.00	1.00	1.00	1.00	1.00	1.00	1.00	1.00
60	1.00	1.00	1.00	1.00	1.00	1.00	1.00	1.00	1.00	1.00
75	1.00	1.00	1.00	1.00	1.00	1.00	1.00	1.00	1.00	1.00
90	1.00	1.00	1.00	1.00	1.00	1.00	1.00	1.00	1.00	1.00
					AR-0.50					
0	1.35	1.25	1.20	1.30	1.47	2.00	1.36	1.28	1.35	1.72
15	1.06	1.10	1.15	1.29	1.50	1.50	1.18	1.24	1.40	1.83
30	1.00	1.00	1.07	1.29	1.36	1.00	1.08	1.16	1.41	1.60
45	1.00	1.00	1.00	1.00	1.00	1.00	1.00	1.04	1.06	1.20
60	1.00	1.00	1.00	1.00	1.00	1.00	1.00	1.00	1.00	1.00
75	1.00	1.00	1.00	1.00	1.00	1.00	1.00	1.00	1.00	1.00
90	1.00	1.00	1.00	1.00	1.00	1.00	1.00	1.00	1.00	1.00
					AR-1.0					
0	1.40	1.22	1.35	1.42	1.50	1.92	1.27	1.58	1.96	2.00
15	1.15	1.13	1.23	1.32	1.50	1.69	1.38	1.38	1.80	2.00
30	1.07	1.00	1.00	1.21	1.38	1.43	1.28	1.15	1.64	2.00
45	1.02	1.00	1.00	1.10	1.13	1.20	1.05	1.00	1.48	1.61
60	1.00	1.00	1.00	1.00	1.00	1.00	1.00	1.00	1.32	1.25
75	1.00	1.00	1.00	1.00	1.00	1.00	1.00	1.00	1.16	1.00
90	1.00	1.00	1.00	1.00	1.00	1.00	1.00	1.00	1.00	1.00
					AR-2.0					
0	1.42	1.50	1.50	1.50	1.50	1.92	1.77	1.97	1.92	1.90
15	1.31	1.41	1.27	1.39	1.50	1.70	1.95	1.75	1.77	2.00
30	1.17	1.00	1.03	1.27	1.45	1.47	1.65	1.57	1.62	2.10
45	1.03	1.00	1.00	1.14	1.23	1.25	1.32	1.27	1.47	1.95
60	1.00	1.00	1.00	1.00	1.00	1.02	1.00	1.02	1.32	1.62
75	1.00	1.00	1.00	1.00	1.00	1.00	1.00	1.00	1.17	1.32
90	1.00	1.00	1.00	1.00	1.00	1.00	1.00	1.00	1.00	1.00
					AR-4.0					
0	1.50	1.50	1.50	1.50	1.50	2.00	1.90	2.00	2.00	2.00
15	1.33	1.41	1.27	1.39	1.50	1.70	1.95	1.75	1.77	2.00
30	1.17	1.00	1.03	1.27	1.45	1.47	1.65	1.57	1.62	2.00
45	1.03	1.00	1.00	1.14	1.23	1.25	1.32	1.27	1.47	1.95
60	1.00	1.00	1.00	1.00	1.00	1.02	1.00	1.02	1.32	1.62
75	1.00	1.00	1.00	1.00	1.00	1.00	1.00	1.00	1.17	1.32
90	1.00	1.00	1.00	1.00	1.00	1.00	1.00	1.00	1.00	1.00

exactly as Eq. (23) for trailing-edge bluntness effects. That is,

$$C_{M_\alpha} = \left(C_{M_\alpha}\right)_0 [1 + f_1(h/c, M)\, f_2(r_{\mathrm{LE}}/t) \times f_3(AR)\, f_4(N_F)\, (h/c)\, /(t/c)] \tag{23}$$

The effect of Eqs. (18) and (23) on the overall configuration aerodynamics will, thus, be to add a slight amount of normal force and pitching moment coefficient to a wing with blunt trailing edges. If this wing is located at the rear of the configuration, it will have a stabilizing effect on the vehicle. This stabilizing effect will be the strongest at the higher Mach numbers. On the other hand, if the wing is at the front of the vehicle, the effect will be destabilizing.

Results and Discussion

We will now attempt to validate the predicted effect of trailing-edge bluntness on the normal force of wings through Eq. (18), along with the center of pressure of a configuration that uses Eqs. (18) and (23). However, before the normal force and center of pressure are investigated, the AP02 axial force coefficient accuracy will be assessed for wings that have blunt trailing edges or truncated leading edges. One configuration used for the axial force assessment is taken from Ref. 7 and is shown in Fig. 6a. Reference 7 gave actual flight-test results based on doppler radar of the body–tail configuration and wing–body–tail configuration of Fig. 6a where the wing trailing edge varied from being sharp to fully blunt. Figure 6b compares the predictions of the AP02 to the experimental data for Ref. 7 for the body–tail case and the wing–body–tail where the wing trailing edge is sharp and 100% blunt. As seen in Fig. 6b, the AP02 gives reasonably good predictions of axial force coefficient for the body–tail case and the wing–body–tail case when the wing trailing edge is sharp. However, for the wing–body–tail case where the wing is 100% blunt, the AP02 predictions deviate from the flight data for Mach numbers below about 1.3.

In the assessment of the reason for the underprediction of the AP02 axial force coefficient for Mach numbers below about 1.3, it was concluded the two-dimensional base pressure coefficient the AP02 uses was too low in this Mach number region. As a result, the next version of the APC (anticipated to be the AP05) will utilize improved values of $C_{P_{2\text{-}D}}$ for Mach numbers below 1.3 in computing wing drag. The new values of $C_{P_{2\text{-}D}}$ compared to the values in the AP02 are shown in Table 2. By the utilization of the improved values of $C_{P_{2\text{-}D}}$ in the AP02, the improved axial force predictions in Fig. 6b are shown as AP05. The average axial force accuracy is now within the $\pm 10\%$ range for the AP05 for all three cases considered in Fig. 6b.

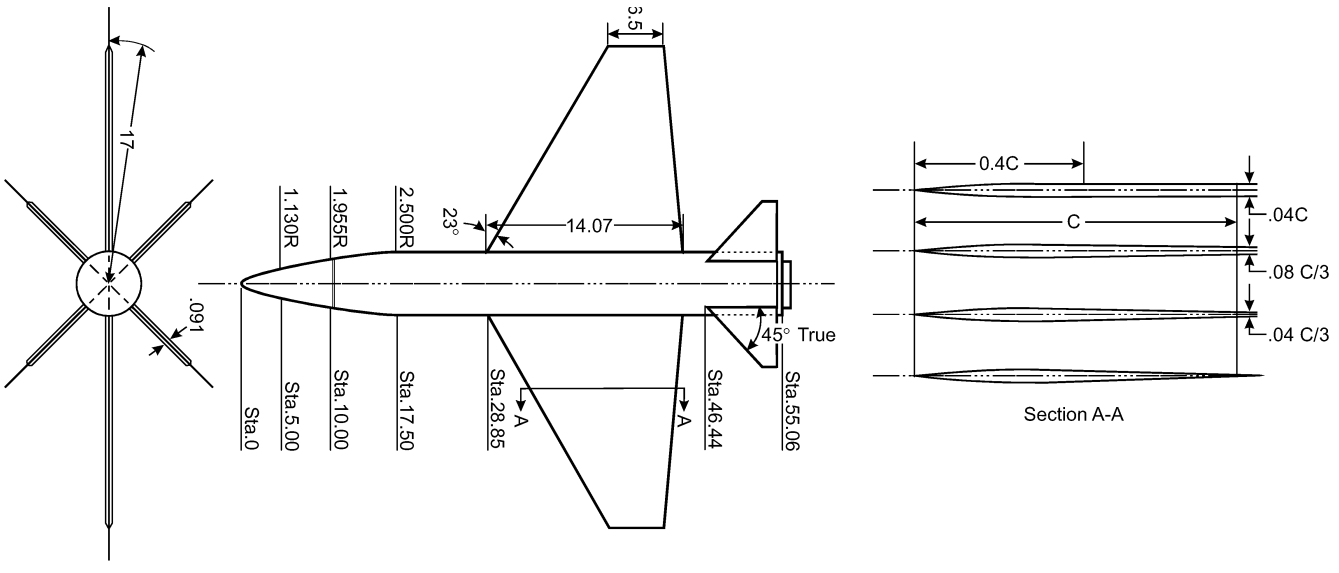

Fig. 6a General arrangements of vehicle showing each airfoil section investigated (from Ref. 7).

Table 2 Improved values of the two-dimensional base pressure coefficient for the AP05

	$C_{P_{2\text{-}D}}$	
M	AP02	AP05
0.00	0.240	0.430
0.50	0.260	0.430
0.70	0.285	0.430
0.80	0.305	0.450
0.85	0.325	0.480
0.90	0.345	0.520
1.00	0.440	0.610
1.05	0.435	0.580
1.10	0.430	0.550
1.20	0.420	0.450
1.30	0.390	0.390
1.50	0.337	0.337
1.70	0.285	0.285
1.90	0.245	0.245
2.10	0.213	0.213
2.30	0.186	0.186
2.50	0.165	0.165
2.80	0.115	0.115
3.10	0.095	0.095
3.70	0.078	0.078
4.00	0.070	0.070
4.30	0.055	0.055

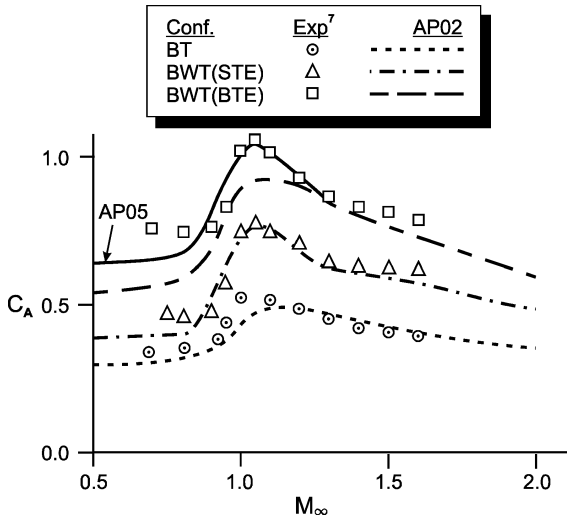

Fig. 6b Comparison of theory and experiment to Fig. 6a configuration.

The second configuration to assess the accuracy of the axial force coefficient prediction is taken from the Aeroballistic Research Facility data of Ref. 14. Reference 14 tests include circular, elliptic, triangular, and square cross-sectional shapes. Figure 7a shows the configurations tested. The fins of the Ref. 14 tests had 100% truncated leading and trailing edges of $0.032d$ thickness. Figure 7b shows the AP02 theoretical results along with the improvements in the Table 2 $C_{P_{2-D}}$ results (AP02 + TEB). Although the Table 2 results help to improve the comparison of the theory to experiment slightly for Mach numbers below 1.2, the theory is still low for Mach numbers below about 1.0. The reason for this is that, whereas for supersonic speeds the AP02 computes the wave drag of the flat faced wings fairly accurately, for transonic speeds the AP02 assumes the wave drag varies from its value at $M = 1.05$ to 0.0 at $M = 0.85$. Hoerner[15] shows a drag coefficient of about 1.0 for a flat faced shape like the wing of Fig. 7a. Subtracting off the base and skin-friction drag terms, one is still left with a value of about 0.5 for the axial force coefficient of the forward face (based on wing frontal area). Hence, this term must be accounted for in the AP05.

An approximate method to account for the axial force coefficient on the truncated leading edge of a wing is given by

$$C_{A_{\text{LE}}} = 0.5 C_{P_0} (A_{\text{BLE}}/A_{\text{ref}}) \tag{24}$$

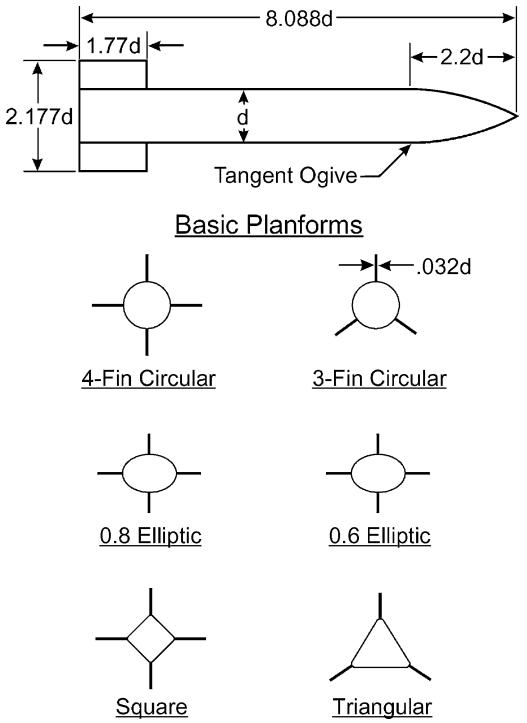

Fig. 7a Model cross-section configurations tested at U.S. Air Force Research Laboratory.[14]

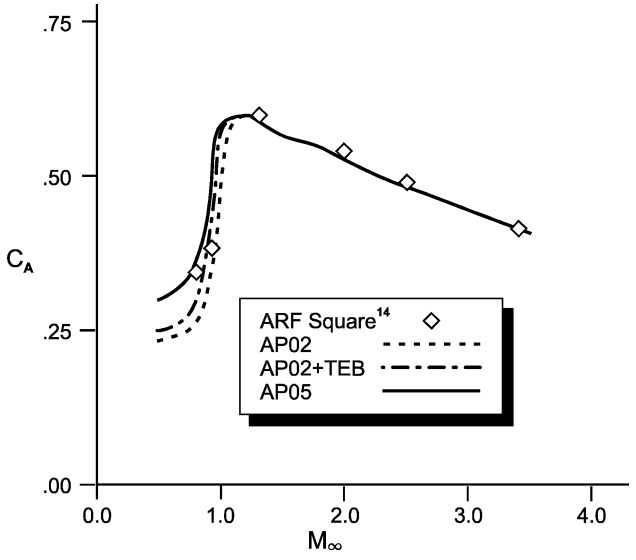

Fig. 7b Comparison of theory to square cross section axial force coefficient data.

C_{P_0} of Eq. (24) can be computed from

$$C_{P_0} = \left(2/\gamma M_\infty^2\right)\left(\left\{1 + [(\gamma - 1)/2]M_\infty^2\right\}^{\gamma/(\gamma-1)} - 1\right) \tag{25}$$

A_{BLE} is the frontal area of the flat faced portion of the wing. Using Eqs. (24) and (25), one obtains the results in Fig. 7b shown as the AP05. Equations (24) and (25) will be integrated into the AP02 code for Mach numbers 0.85 and below. For Mach numbers between 1.05 and 0.85, linear interpolation is used between the AP02 values for the wing wave drag at $M = 1.05$ and the value computed by Eqs. (24) and (25) at $M = 0.85$. Note that if the wing leading edge is rounded vs being truncated, no appreciable pressure drag occurs on the leading edge according to Ref. 15. The current version of the AP02 will give good results for sharp or rounded leading-edge wings, and so no modifications are needed for these wing shapes.

The last configuration to compare the new axial force prediction of the improvements to the AP02 is shown in Fig. 8a. This configuration is a typical guided projectile concept with eight tail fins for stability. It is 12.17 calibers in length with a low drag nose and a boattail. The unpublished wind-tunnel test data (provided to API by S. Renaldi of NSWCDD) was for fins with a single wedge, except at $M_\infty = 3.5$, where both single and double wedge fins were tested. The fin cross-sectional shapes are shown in Fig. 8a. Figure 8b compares the AP02 predictions for both the single and double wedge cases to the single wedge experimental data. The double wedge axial force experimental data at $M = 3.5$ was approximately the same as the single wedge value. Note the improved two-dimensional base pressure values of Table 2 that will be in the AP05 show improved comparison to experiment for $M_\infty < 1.3$. In general, good agreement with experiment is seen, particularly with the AP05.

We are now ready to validate the new method of predicting trailing-edge bluntness on the normal force coefficient and center of pressure as defined by Eqs. (18) and (23). The first case considered is the Fig. 8a case. Figures 8c and 8d compare the theory to experiment for both the normal force coefficient derivative and center of pressure. The values shown in Figs. 8c and 8d were derived based on experimental data of ±2 deg AOA and the AP02 and AP05 calculations were performed at 2 deg AOA also. Note in Figs. 8c and 8d that the AP02 gives the same values for C_{N_α} and X_{CP} for the single and double wedge fins, whereas the AP05 will show improvements in predictions for both the single and double wedge. The double wedge improvements come from adding an aspect ratio 4 table in Table 1, whereas the AP02 uses aspect ratio 2 data for

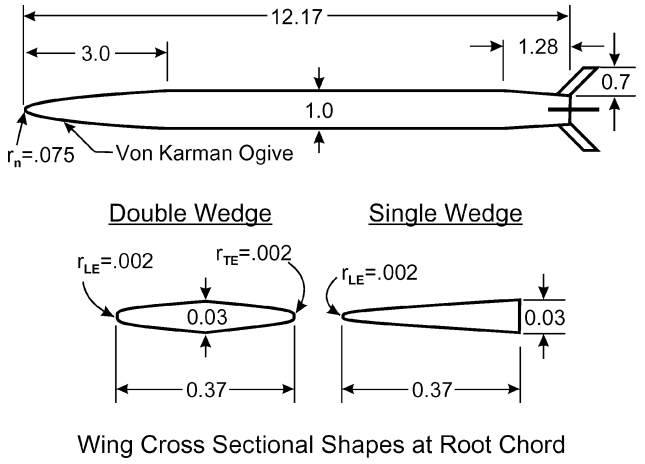

Fig. 8a Eight-fin guided projectile concept (dimensions in calibers).

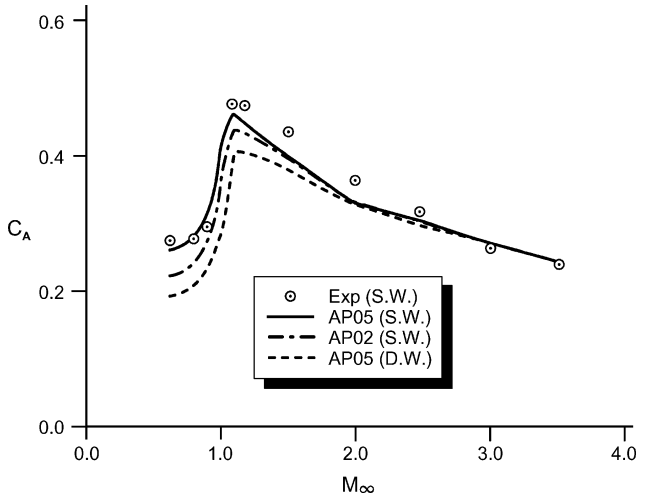

Fig. 8b Axial force coefficient vs Mach number for Fig. 8a configuration.

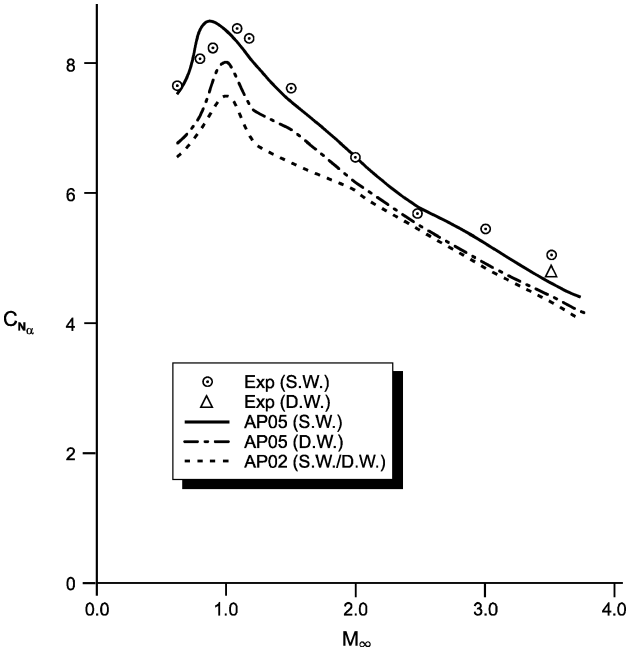

Fig. 8c Normal force coefficient derivative for Fig. 8a configuration.

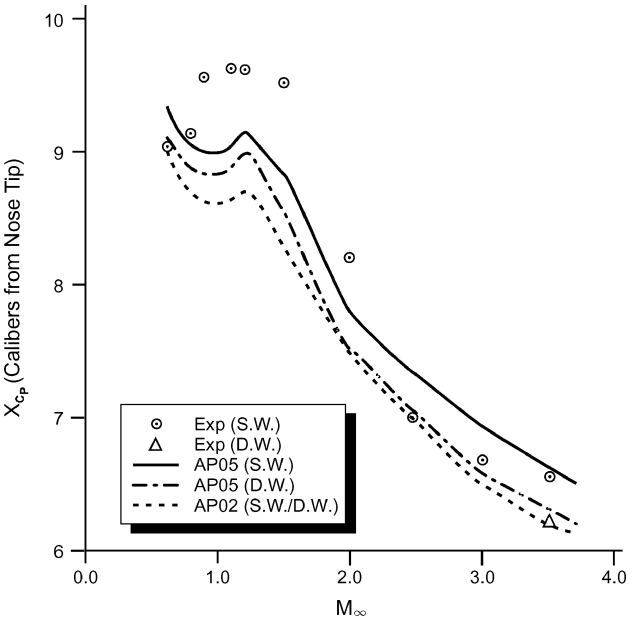

Fig. 8d Center of pressure for Fig. 8a configuration.

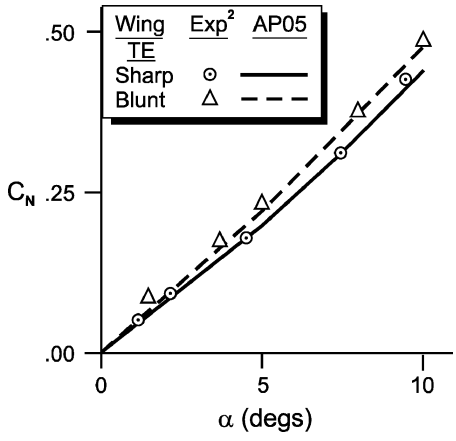

Fig. 9 Normal force coefficient of wing alone ($AR = 4.0$, $\lambda = 1.0$, and $M_\infty = 2.0$).

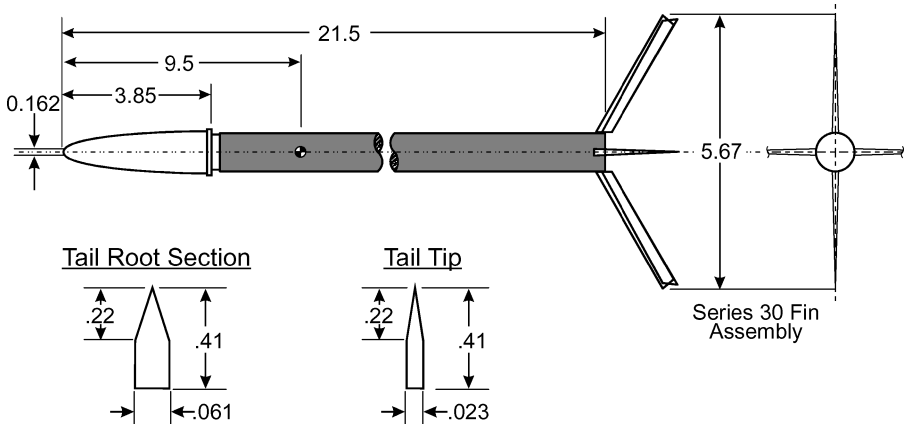

Fig. 10a Body–tail configuration tested in Ref. 4 (dimensions in calibers).

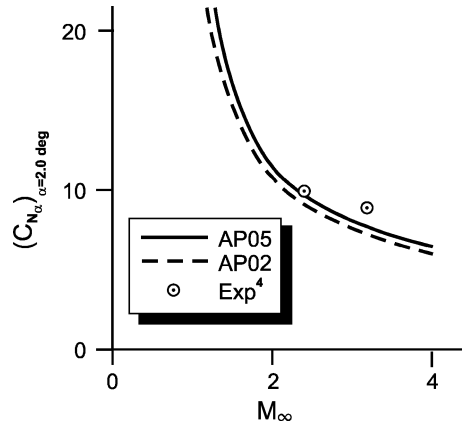

Fig. 10b Theoretical and experimental comparisons of C_{N_α}.

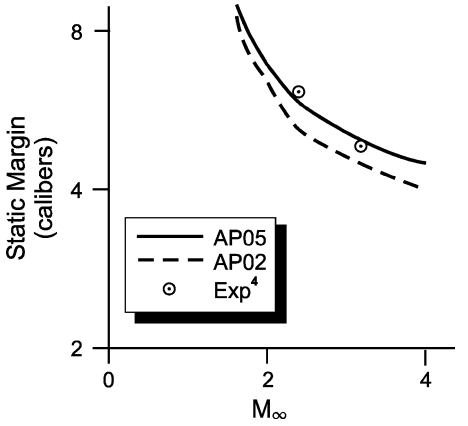

Fig. 10c Theoretical and experimental comparison of static margin at $\alpha = 2$ deg.

all aspect ratios 2.0 and greater. The single wedge improvements in Figs. 8c and 8d come from both the Table 1 extension and the new methods of Eqs. (18) and (23). In general, the improvements to be a part of the AP05 show improvement compared to experiment over the AP02. The AP05 shows good agreement to experiment for C_{N_α}. The center of pressure is predicted too far forward by about one-half a caliber at transonic speeds. Of particular importance is the comparison of the AP05 single and double wedge data to experiment at Mach 3.5. Whereas the absolute value of the theory is off slightly for both C_{N_α} and X_{CP}, the magnitude of the experimental difference between the single and double wedge is predicted quite well. Unfortunately, experimental data for the double wedge were unavailable for Mach numbers other than 3.5.

The next case considered is a wing alone case from Ref. 2 with an aspect ratio of 4.0, taper ratio of 1.0, and Mach number of 2.0. AP05 comparisons of theoretical normal force coefficient to experiment for both the sharp and blunt trailing-edge cases are shown in Fig. 9. Good comparison of theory to experiment is seen for both cases.

The third case considered is taken from Ref. 4. The configuration tested is 21.5 calibers in length with a 3.85-caliber nose with a truncated tip radius of 0.162. The fins have an aspect ratio of 11.4. The case considered has a wedge leading edge with a blunt trailing edge. The wing has a thickness ratio (t/c) of 0.15 at the root and 0.05 at the tip. It is sweptback 30 deg. Figure 10a shows the configuration along with the airfoil cross-sectional shape. Figures 10b and 10c compare the AP02, along with the improvements added to the AP02 (denoted as AP05) to the Ref. 4 experimental data for C_{N_α} and X_{CP}. Data were available only for $M = 2.48$ and 3.24. For these two data points, the AP05 is in closer agreement to experiment than the AP02. The center of pressure prediction errors are less than 1% of the body length for both Mach numbers. The AP05 C_{N_α} predictions are also within the $\pm 10\%$ accuracy goal of the APC.

Summary

To summarize, a new semi-empirical method has been developed to estimate the effects of wing trailing-edge bluntness on the normal force, pitching moment, and center of pressure at low AOA. The low AOA aerodynamics methods are combined with existing, well-validated nonlinear methods for high AOA aerodynamics. Comparisons of the new method to experimental data at low AOA show the improvements added to the AP02 will allow the next version of the APC (anticipated to be the AP05) to have improved accuracy over the AP02 when the wings have truncated trailing edges.

In addition to the new method to predict the effect of trailing-edge bluntness on the lift properties at low AOA, several other refinements were found to give improved accuracy in wing aerodynamics at transonic and subsonic Mach numbers. These refinements include improvements in the two-dimensional base pressure coefficient, an approximate method to estimate pressure drag on the leading edge of fins when the leading edge is truncated, and reduction of the effect of wing thickness on the wing lift properties at transonic speed.

Acknowledgment

Appreciation is given to John Fraysse of the U.S. Naval Surface Warfare Center, Dahlgren, Virginia, for providing the funding support to allow this work to be performed.

References

[1]Moore, F. G., and Hymer, T. C., "2002 Version of the Aeroprediction Code (AP02)," *Journal of Spacecraft and Rockets*, Vol. 41, No. 2, 2004, pp. 232–247; also AIAA Paper 2003-0026, Jan. 2003.

[2]Chapman, D. R., and Kester, R. H., "Effect of Trailing-Edge Thickness on Lift at Supersonic Speeds," NACA RM A52D17, July 1952.

[3]Luther, M. L., Jaeger, B. F., and Schroedter, G. M., "The Lift and Center of Pressure at Supersonic Speeds of Blunt-Trailing-Edge Airfoils with

and Without Sweepback," NAVORD Rept. 1288 (NOTS 358), (DTIC AD B183433), Defense Technical Information Center, Ft. Belvoir, VA, Feb. 1951.

[4]Jaeger, B. F., Luther, M. L., and Schroedter, G. M., "The Aerodynamic Characteristics at Supersonic Speeds of Blunt-Trailing-Edge Airfoils for the NOTS Small-Caliber Air-to-Air Folding-Fin Rocket," NAVORD Rept. 1287 (NOTS 357), (DTIC AD B954298), Defense Technical Information Center, Ft. Belvoir, VA, Feb. 1951.

[5]Busemann, V. A., and Walchmer, G., "Airfoil Characteristics at Supersonic Speeds," *Forschung auf dem Gebiete des Ingenieurwesons*, Vol. 4, No. 2, 1933, pp. 87–92.

[6]Jaeger, B. F., Luther, M. L., and Schroedter, G. M., "The Aerodynamic Characteristics at High Subsonic Speeds of Blunt-Trailing-Edge Airfoils for the NOTS Small-Caliber Air-to-Air Folding-Fin Rocket," NAVORD Rept. 1289, China Lake, CA, Feb. 1951.

[7]Morrow, J. D., "Measurements of the Effect of Trailing-Edge Thickness on the Zero-Lift Drag of Thin Low-Aspect-Ratio Wings," NACA TN 3550, Nov. 1955.

[8]Chapman, D. R., Wimbrow, W. R., and Kester, R. H., "Experimental Investigation of Base Pressure on Blunt-Trailing-Edge Wings at Supersonic Velocities," NACA Rept. 1109, 1952.

[9]Chapman, D. R., "Reduction of Profile Drag at Supersonic Velocities by the Use of Airfoil Sections Having a Blunt Trailing Edge," NACA RM A9H11, Nov. 1949.

[10]Chapman, D. R., "Airfoil Profiles for Minimum Pressure Drag at Supersonic Velocities—Application of Shock-Expansion Theory, Including Consideration of Hypersonic Range," NACA TN 2787, Sept. 1952.

[11]Moore, F. G., *Approximate Methods for Weapon Aerodynamics*, Vol. 186, Progress in Astronautics and Aeronautics, AIAA, Reston, VA, 2000, Chaps. 3 and 4.

[12]"Equations, Tables, and Charts for Compressible Flow," NACA Rept. 1135, 1953.

[13]Moore, F. G., McInville, R. M., and Robinson, D. I., "A Simplified Method for Predicting Aerodynamics of Multi-Fin Weapons," U.S. Naval Surface Warfare Center, NSWCDD/TR-99/19, Dahlgren, VA, March 1999.

[14]Hathaway, W. H., Kruggel, B., Abate, G., Winchenbach, G., and Krieger, J., "Aeroballistic Range Tests of Missile Configurations with Noncircular Cross Sections," U.S. Air Force Research Laboratory Munitions Directorate, AFRL-MN-EG-TR-2001-7082, Eglin AFB, FL, Sept. 2001.

[15]Hoerner, S. F., "Fluid Dynamics Drag," Hoerner Fluid Dynamics, Brick Town, NJ, 1965, pp. 3–12.

M. Miller
Associate Editor